Asymmetric Pore Distribution and Loss of Membrane Lipid in Electroporated DOPC Vesicles

Ephrem Tekle,* R. D. Astumian,† W. A. Friauf,‡ and P. B. Chock*

*Laboratory of Biochemistry, National Heart, Lung, and Blood Institute, and ‡Division of Bioengineering and Physical Sciences, National Institutes of Health, Bethesda, Maryland 20892, and †Department of Surgery, Section of Plastic and Reconstructive Surgery, University of Chicago, Chicago, Illinois 60637 USA

ABSTRACT An externally applied electric field across vesicles leads to transient perforation of the membrane. The distribution and lifetime of these pores was examined using 1,2-di-oleoyl-*sn*-glycero-3-phosphocholine (DOPC) phospholipid vesicles using a standard fluorescent microscope. The vesicle membrane was stained with a fluorescent membrane dye, and upon field application, a single membrane pore as large as ~7 μm in diameter was observed at the vesicle membrane facing the negative electrode. At the anode-facing hemisphere, large and visible pores are seldom found, but formation of many small pores is implicated by the data. Analysis of pre- and post-field fluorescent vesicle images, as well as images from negatively stained electron micrographs, indicate that pore formation is associated with a partial loss of the phospholipid bilayer from the vesicle membrane. Up to ~14% of the membrane surface could be lost due to pore formation. Interestingly, despite a clear difference in the size distribution of the pores observed, the effective porous areas at both hemispheres was approximately equal. Ca^{2+} influx measurements into perforated vesicles further showed that pores are essentially resealed within ~165 ms after the pulse. The pore distribution found in this study is in line with an earlier hypothesis (E. Tekle, R. D. Astumian, and P. B. Chock, 1994, *Proc. Natl. Acad. Sci. U.S.A.* 91:11512–11516) of asymmetric pore distribution based on selective transport of various fluorescent markers across electroporated membranes.

INTRODUCTION

External electric fields of short duration across intact cells and vesicular systems leads to transient membrane pores through which influx/efflux of impermeable molecules is believed to occur (Zimmermann, 1986; Neumann et al., 1989; Chang et al., 1992; Potter, 1988). These events are generally referred to as electroporation or electropermeabilization and have led to a number of other related processes such as electrofusion for the production of somatic cell hybrids (Al-Atabee et al., 1990) and electroinsertion for the specific incorporation of proteins in cellular membranes (Mouneimne et al., 1991) as well as recent clinical applications in targeted transdermal drug delivery and tumor treatment (Prausnitz et al., 1993; Heller et al., 1996). The induction of pores on the membrane surface of some given number, size(s), and lifetime(s) is one common feature underlying all these processes and ultimately governs the relative success of the various methods used. Consequently, significant focus has been directed toward a basic understanding of the underlying mechanisms involved.

Field-induced membrane pores have been reported on a number of cell types under a variety of experimental conditions, e.g., red blood cells and ghosts (Chang and Reese, 1990; Sowers and Lieber, 1986; Sowers, 1987), mammalian and plant cells (Tekle et al., 1990, 1991, 1994; Gabriel and Teissie, 1997; Mehrle et al., 1985, 1989), sea urchin eggs (Hibino et al., 1991, 1993; Kinosita et al., 1988), and bacterial cells (Miller et al., 1988). Irrespective of the cell type examined to date, by far the most consistent finding has been the eminent rupture of the membrane provided a critical transmembrane potential, $\Delta\phi_c$ (~0.3–1 V), develops across the membrane, where $\Delta\phi_c$ refers to the minimum amplitude required for macroscopically observable electroporation. For non-porated membranes, the magnitude of the sub-critical transmembrane potential, $\Delta\phi_i$, due to an external electric field, E, is given by (Neumann and Rosenheck, 1973)

$$\Delta\phi_i = (3/2)b\,E\cos(\theta), \tag{1}$$

where b is the outer radii of the cell membrane and θ is the angle between the field direction and any point on the membrane. The maximum potential drop at the poles of the membrane facing the electrodes (i.e., $\cos(\theta) = \pm 1$ at $\theta = \pi$, 0) and the cosine dependence have generally been confirmed by a number of studies employing potential-sensitive dyes (Ehrenberg et al., 1987).

By contrast, the density of these pores as well as their size and distribution on the perforated membrane surface is less well understood, and their structure is even far less known. One clear exception to the latter is an earlier study by Chang and Reese (1990) where a rapid freezing electron microscopy was used to show volcano-shaped pores in erythrocyte membranes exposed to an intense electric pulse. These pore structures were visually detectable ~3 ms after the pulse and resealed to their initial state in several seconds with no observable residue. The spatial disposition of the pores relative to the electroporating pulse was, however, not re-

Received for publication 11 July 2000 and in final form 2 May 2001.

Address reprint requests to Dr. E. Tekle, Laboratory of Biochemistry, NHLBI, NIH, 50 South Drive, Room 2127, MSC 8012, Bethesda, MD 20892-8012. Tel.: 301-496-8390; Fax: 301-496-0599; E-mail: ephrem@helix.nih.gov.

0006-3495/01/08/960/09 $2.00

solved. Nevertheless, based on these early findings and further modeling studies (Weaver and Barnett, 1992; Kakorin et al., 1996), it is currently thought the initial electroporation event involves the rearrangement of clusters of lipids into hydrophobic and hydrophilic pore structures with minimum pore size in the order of a few nanometers. Estimates of the number of pores per cell, derived from conductance and transport studies, have ranged from just a few (<10) (Saulis et al., 1991), ~700 (Sowers and Lieber, 1986) pores in ghost cells to up to $\sim 10^5$ in mouse B cells (Neumann et al., 1998). Percolation of these nanometer-sized primary pores into larger openings have also been envisaged (Sugar and Neumann, 1984). Much of the insight into how and where these pores are distributed on the membrane surface has largely been inferred from transport studies involving influx/efflux of probe molecules (Dimitrov and Sowers, 1990; Tekle et al., 1990; Mehrle et al., 1989; Gabriel and Teissie, 1998) as well as from optical signals of membrane-bound potential-sensitive dyes (Hibino et al., 1991, 1993; Kinosita et al., 1988). Some features of the experimentally observed permeabilization patterns have recently been shown in a series of modeling studies of asymmetric electroporation (DeBruin and Krassowska, 1999a,b). However, although influx/efflux and sieving experiments are powerful methods in probing membrane pore dynamics, it is crucial to note these approaches may not necessarily indicate the type of pores created or how they may have distributed at the membrane level, as the overall transport process could depend on the nature of the probe molecules used, the mode of transport, and the kinetics of pore closure, all of which, or in some combination, could lead to potential misinterpretations. This possible anomaly, for instance, was originally anticipated by Saulis (1993) in a modeling study of asymmetric electroporation. Our earlier study (Tekle et al., 1994) had also shown selective transport of various fluorescent markers on one side of the membrane despite the fact that both hemispheres of cell membrane were permeabilized. This earlier finding implied structurally different pores may have formed at the opposite poles of the membrane, although no direct experimental evidence was available in support of the hypothesis. It is thus clear that current views on the structure, dynamics, and density of field-induced membrane pores are limited, and further studies with a particular focus to events occurring at the membrane level would be useful. In this respect, vesicles offer a relatively less complex membrane structure and have been used as model systems in a few earlier studies (Teissie and Tsong, 1981; Zhelev and Needham, 1993), including more recent ones (Tonsing et al., 1997; Kakorin et al., 1998; Kakorin and Neumann, 1998). Small unilamellar vesicles (SUVs, diameter ~100 nm) were employed in these studies, and no spatial information was thus obtained.

Here, giant vesicles (diameter >10 μm) of 1,2-di-oleoyl-*sn*-glycero-3-phosphocholine (DOPC) were used to monitor the induction and distribution of pores at the membrane level. A combination of membrane staining, electron microscopy, and Ca^{2+} influx measurements were employed to study the overall dynamics. The results revealed single visible pores (on the order of ~7 μm) are predominantly formed at the cathode-facing hemisphere and many small pores at the anode-facing hemisphere. Analysis of the fluorescence pattern of the stained membrane as well as electron micrographs of negatively stained vesicles shows pore formation is accompanied by loss of lipid from the membrane surface. Despite the difference in the pore size distribution, however, the overall porous area at both vesicle hemispheres was found to be comparable. The pores are resealed within a few hundred milliseconds after the pulse. These findings are compared and discussed with currently held views on asymmetric electroporation.

MATERIALS AND METHODS

Reagents

DOPC in chloroform was purchased from Avanti Polar Lipids (Alabaster, AL). 1-(3-sulfonatopropyl)-4-[B][2-(d*i*-*n*-butylamino)-6-naphthyl vinyl] pyridinium betaine (Di-4-ANEPPS) and Fluo-3 penta-ammonium salt were from Molecular Probes (Eugene, OR). $CaCl_2$ was from Fisher (St Louis, MO).

Preparation of vesicles

Vesicles were prepared following the procedure of Angelova et al. (1992) using low-amplitude AC fields and modified to allow exchange of hydrating liquid. A chamber was constructed using two conducting indium-tin-oxide-coated microscope cover glasses (Delta Technologies, Stillwater, MN), separated with a 1-mm-thick Teflon spacer and was fitted with a simple flow system to allow exchange of hydrating liquids. A 2-μl sample from a 20 mg/ml stock solution of DOPC in chloroform was placed on the upper glass electrode and dried extensively under a stream of nitrogen. The chamber was then reassembled and the lipid hydrated using either deionized water alone or a solution containing the desired dyes, i.e., di-4-ANEPPS or Fluo-3. The initial hydration was done by directly injecting 200 μl of the solution near the dried lipid with a micropipette. An AC field of ~70 V/cm, frequency 5 Hz, was then applied across the chamber from a waveform generator (WaveTek 183, San Diego, CA), and the formation of the vesicles was monitored under the microscope (Zeiss, Axiovert 100). Within ~1 h, several layers of large vesicles, diameter ~25 μm, were formed on the surface of the hydrated lipid. Inner layers contained progressively smaller vesicles that grew with time up to ~2 h. Before the removal of the vesicles, the bathing solution was replaced with dye-free medium to remove unincorporated dye. Membrane labeling with di-4-ANEPPS was primarily done after the vesicles have formed by bathing the vesicles in a solution containing the dye, unless stated otherwise. The larger vesicles on the outer layer were finally collected by gentle agitation of the bathing solution with a micropipette. Typical yield of vesicles of diameter b, 20 μm < b < 30 μm, was 200–300 per 100 μl of solution. These vesicle preparations were stable for several days at 4°C. In all the experiments reported here, the outside concentrations of the reagents used were, 5 μM di-4-ANEPPS, 25 μM Fluo-3, and 2.5 mM $CaCl_2$.

Electroporation and image acquisition equipment

The electroporation and image acquisition system is similar to that described previously (Tekle et al., 1991, 1994). Electric pulses of desired

amplitude and a pulse width were supplied from a high-power pulse generator (model 360, Velonex, Santa Clara, CA) and applied across vesicles placed in an electroporation chamber. The chamber was constructed with two polished stainless steel electrodes, fixed on a 75- × 25-mm microscope glass slide. The inter-electrode separation was 1 mm. The amplitude and pulse widths for each experiment were monitored across the chamber on a digital oscilloscope (54502A, Hewlett-Packard, Palo Alto, CA) using a 100:1 probe. The chamber is mounted on an inverted fluorescence microscope (Zeiss, Axiovert-100), and the excitation and emission wavelengths were set with appropriate bandpass and cutoff filters at 520 and 610 nm for red emission and 480 and 520 for green emission, respectively. Fluorescence images were acquired with an intensified camera (SIT-68, DAGE-MTI, Michigan City, IN) and recorded onto a VHS tape (Panasonic model AG-7350). The intensity of the fluorescence emissions was also monitored on an analog scope (Hitachi, V-212) to protect the camera from excessive light exposure as well as to monitor against saturation of the measured signals. Images were later processed using the National Institutes of Health Image 1.62 software (National Institutes of Health, Bethesda, MD) on a PowerMac 9500 computer. Because the electroporation events were fast and often complete within only a few video frames, it was necessary to identify $t = 0$ by synchronizing the video signal with the rising edge of the electroporating pulse to eliminate timing uncertainty. A useful pulse/video synchronization circuit was built for this purpose (circuit diagram available upon request). The trigger signal is the odd/even field signal from an LM 1881 sync separator (National Semiconductor, Santa Clara, CA), which is driven by the composite video signal from the video camera. When this flip-flop is triggered, it provides an output to the pulse generator to start the experiment in synchrony with the video signal. The circuit is further designed to stamp a bright vertical bar near the upper left corner of the video image and vanishes at the instant of the output trigger. This triggering system accurately locates the video frame in which the electric pulse is applied so that the time of electric pulse application is included on the video frame recording of the experiment. Successive video frames could then be time resolved at 33 ms per frame.

Electron microscopy

Vesicle preparations were negatively stained following a similar procedure described by Moscho et al. (1996). Grids coated with a parlodion/carbon substrate were treated with poly-D-lysine (1 mg/ml), rinsed, air dried, and glow discharged just before use to make them hydrophilic. Vesicles were prepared as described earlier here, and a drop of vesicle suspension was placed on Parafilm. The grid was inverted on the drop for ~2 min. Excess liquid was removed by blotting onto a filter paper at the periphery of the grid. The grid was then negatively stained with 3 drops of 1% aqueous uranyl acetate. Excess staining solution was similarly removed using filter paper. Vesicle images were then obtained using a Philips-410 transmission electron microscope at different magnifications.

RESULTS

Our primary aim in this study was to monitor the induction and distribution of field-induced vesicle pores at the membrane level. For this purpose, a widely used potential-sensitive dye, di-4-ANEPPS, was used for its excellent membrane partitioning properties and photo-stability. It should be noted, however, that this dye has been used to monitor fast changes (microseconds time scale) in membrane potential due to externally applied fields (Lojewska et al., 1989), but these optical responses are well below the time resolution (milliseconds time scale) of our equipment here. In the present study, the dye is used as a membrane stain to visualize the rupture events and as a marker for lipid components lost from the vesicle membrane. This stated use is justified given our experimental design and setup.

Fig. 1 shows a typical series of video frames depicting the electroporation events before and after the application of a 1.1-kV/cm (Fig. 1, *A–C*) or 0.920kV/cm in (Fig. 1, *D–F*) field and a pulse width of 700 μs. For all frames, the electrodes are positioned as shown in Fig. 1 *A*. The membrane of the vesicle shown in Fig. 1, *A–C*, was labeled after the vesicle was formed. For the vesicle shown in Fig. 1, *D–F*, the dye was present during vesicle formation so that both the inner and outer leaflets of the membrane were labeled to avoid any asymmetric charge distribution. Fig. 1 *A* is the image before field application, and Fig. 1 *B* shows the first frame (33 ms) after the pulse. It shows that a large pore with a diameter ~6.2 μm was formed at the negative electrode-facing hemisphere, whereas a rare occurrence of a possible visible lipid aggregate loss was seen at the hemisphere facing the anode. In the next frame (66 ms, Fig. 1 *C*), the membrane pore was resealed, partially leaving some of the lipid on the outer surface. In Fig. 1, *D–F*, the time sequence was the same as in Fig. 1, *A–C*, and the pattern of permeabilization is representative of the successful experiments observed. Here again we found a large pore, diameter ~7.5 μm (Fig. 1 *E*), on the side facing the cathode, which subsequently resealed in the next frame, (66 ms, Fig. 1 *F*). These data clearly show that symmetric pores were not created in these vesicle systems. Further experiments and analysis revealed that both sides of the membrane are permeabilized, and a partial loss of membrane lipid occurs as a consequence of pore formation. The asymmetry of electroporation is reflected here in the size distribution of pores at the vesicle hemispheres facing the electrodes. Evidence supporting these events is detailed below.

Based on a number of image data as those shown in Fig. 1, the vesicle dimensions (diameters) were carefully measured before (see for example, Fig. 1, *A* and *D*) and immediately after (Fig. 1, *C* and *F*) the electric field. Vesicle dimensions were measured using contour templates from the vesicle images and are the averages of two readings taken perpendicular to each other. These measurements revealed that a significant reduction occurs in the size of the vesicles after the field and clearly suggest appreciable amount of lipid must have been lost as a result of pore formation. Surprisingly, however, we find that the loss of membrane lipid from the observed pores at the cathode-facing hemispheres (Fig. 1, *B* and *E*) could not account for the extent to which the vesicle size is reduced when measured after the pulse (Fig. 1, *C* and *F*). This discrepancy is elaborated below using the image data in Fig. 1, *D–F*, as an example.

Figure. 2 shows a geometric representation of the image data in Fig. 1 *E*, where r_p is the pore radius and the shaded area, $S = 2\pi r^2(1 - \cos \alpha)$, represents the surface loss due

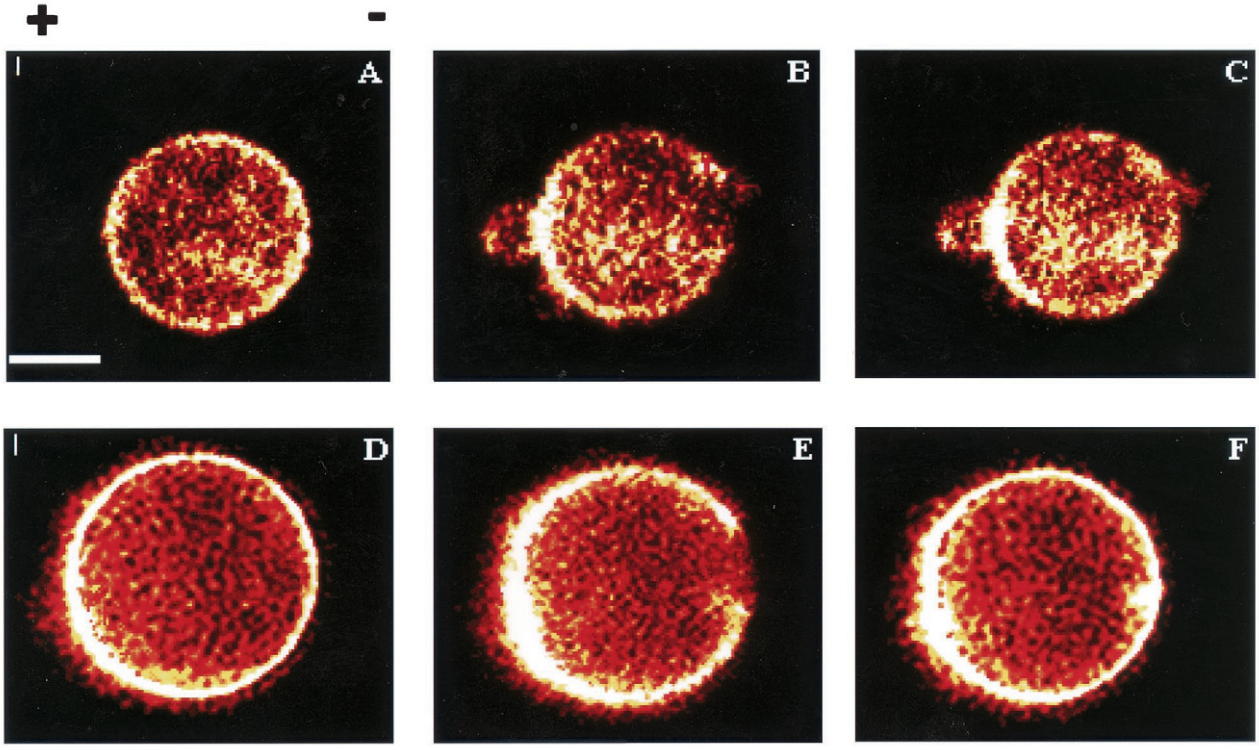

FIGURE 1 A select series of video frames showing the electroporation events before and after electric field application. $E = 1.1$ kV/cm in (*A–C*), and $E = 0.920$ kV/cm in (*D–F*). The pulse width was 700 μs for both cases. The position of the electrodes is as indicated in *A* for all frames. In *A–C*, the membrane was labeled after the vesicle had formed. In *D–F*, the dye was present during vesicle formation so that both the inner and outer leaflets of the membrane are labeled to avoid any asymmetric charge distribution. (*A* and *D*) Images before field application; (*B* and *E*) The first frames (33 ms) after the pulse; (*C–F*) Images at 66 ms after the pulse. The frame images are pseudo colored to enhance visualization of the membrane pores and dye distribution after the field. Scale bar, 10 μm

to pore formation at the cathode-facing hemisphere. If the reduction in vesicle size (Fig. 1 *F*) is solely due to lipid loss at the cathode side, then

$$4\pi r_1^2 - 2\pi r_1^2(1 - \cos\alpha) = 4\pi r_2^2, \tag{2}$$

where r_1 and r_2 are the radii of the vesicles before (Fig. 1 *D*) and after (Fig. 1 *F*) the field, respectively, and α is given by

$$\alpha = \cos^{-1}\left[\frac{2r_2^2}{r_1^2} - 1\right]. \tag{3}$$

The observed pore in Fig. 1 *E* should thus equal r_p, where the pore radius r_p (Fig. 2) is given by

$$r_p = r_1 \sin\alpha. \tag{4}$$

The vesicle radii r_1 (Fig. 1 *D*) and r_2 (Fig. 1 *F*) were measured and found to be 13.4 and 12.7 μm, respectively. Using Eqs. 3 and 4, we find $r_p = 8.1$ μm. However, the pore radius (Fig. 1 *E*) is only ~3.8 μm, about half the value of the computed pore radius, r_p. Table 1 shows further comparisons of the pore radii, r_p, calculated based on measured vesicle sizes before and after the electric pulse with the pore radii observed, r_{obs}, at the cathode-facing hemisphere for

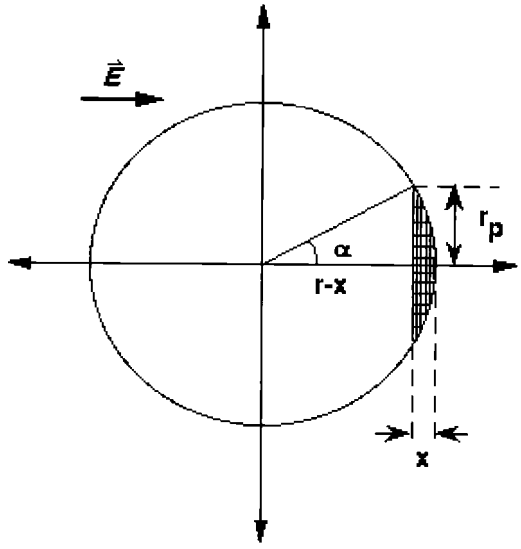

FIGURE 2 Geometrical representation of a vesicle. The shaded area represents the membrane pore as seen in Fig. 1, *B* and *E*. $x = r(1 - \cos\theta)$. The area of the shaded region is $2\pi rx$, where r_p is the pore radius. The electric field is as shown and is directed from left to right.

TABLE 1 Comparisons of pore radii

r_p (μm)	r_{obs} (μm)
7.3	3.1
7.7	4.1
9.6	3.7
6.5	2.7
4.8	2.3

different vesicle preparations. It is interesting to note that the observed pore radii are consistently about half of that of r_p. In terms of total lipid lost from the vesicle membrane, these data suggest at least two possibilities: either 1) additional lipid components must have been lost at other sites on the membrane surface or 2) the pore size at the cathode-facing hemisphere (Fig. 1 *E*) could have been larger at earlier times than can be detected with the current equipment (note that images captured in Fig. 1, *B* and *E*, are ~32 ms after the termination of the external pulse.). The latter possibility seems highly unlikely as it would imply the vesicle would have to lose almost half of its surface on the hemisphere facing the cathode to accommodate a pore radius of ~8.1 μm. More likely, many smaller pores are formed at the anode-facing hemisphere resulting in loss of lipid undetectable by the microscope setup.

Lipid loss at the anode-facing hemisphere is in part implicated based upon the asymmetric distribution of the membrane-staining dye. Before field application, for example, the dye distribution is fairly homogeneous as shown in Fig. 1, *A* and *D*, but a marked asymmetry ensues in the images after the field with increased fluorescence at the anode-facing hemisphere (see Fig. 1, *B*, *C*, *E*, and *F*). These distributions remain for hundreds of seconds after the pulse and could not have been due to potential redistribution around the vesicle as the external field is absent in these time scales. A plausible cause for the uneven dye signal could arise from redistribution of the lipid bilayer itself as a consequence of pore formation such that small lipid aggregates failing to reintegrate to the original bilayer remain attached to the parent vesicle surface. This possibility is supported by electron micrograph images of porated vesicles and explains the persistent enhanced fluorescence long after the pulse has been terminated. The data further point at the site origin of the missing lipid responsible for the observed reduction in the vesicle size shown earlier.

Fig. 3 shows negatively stained electron micrographs of vesicles before (Fig. 3 *A*) and immediately (~2 min) after (Fig. 2, *B* and *C*) electroporation. Fig. 2, *A′*, *B′*, and *C′* are magnified (zoomed) views of the membrane in Fig. 2, *A*, *B*, and *C*, around the area indicated by the arrows. Clearly,

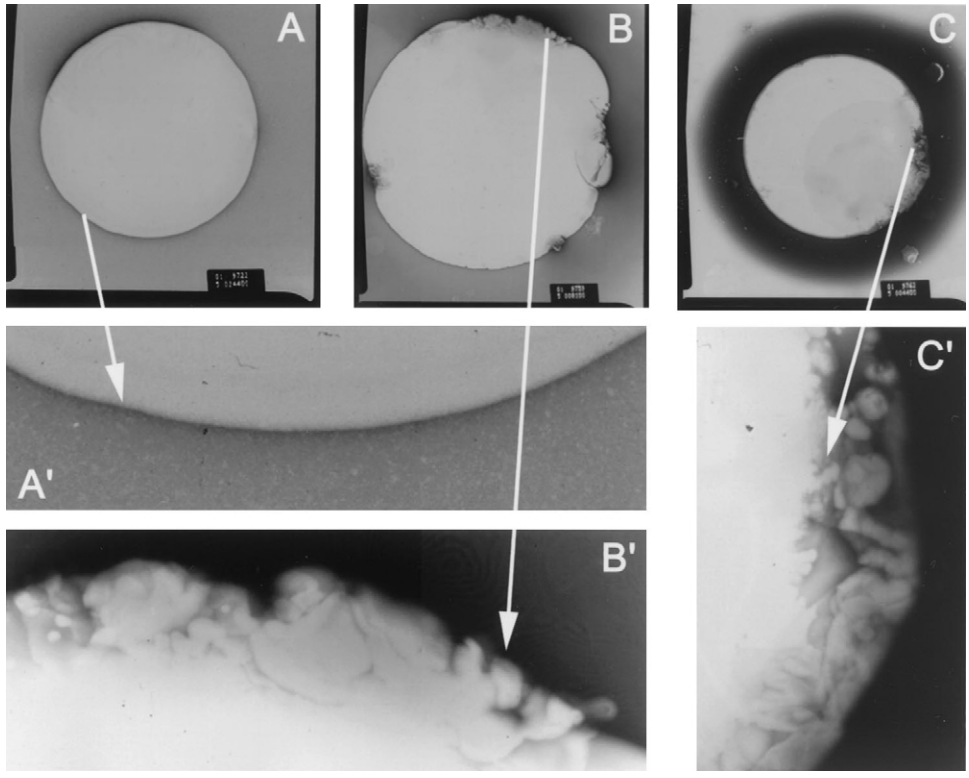

FIGURE 3 Electron micrographs of vesicles stained with 1% uranyl acetate before (*A*) and after (*B*, and *C*) electric field application. $E = 5.7$ kV/cm; pulse width = 700 μs. *A′*, *B′*, and *C′* are magnified views of the area indicated by the arrow. Electron micrograph magnifications: ×24,000 (*A*), ×8700 (*B*), and ×4400 (*C*).

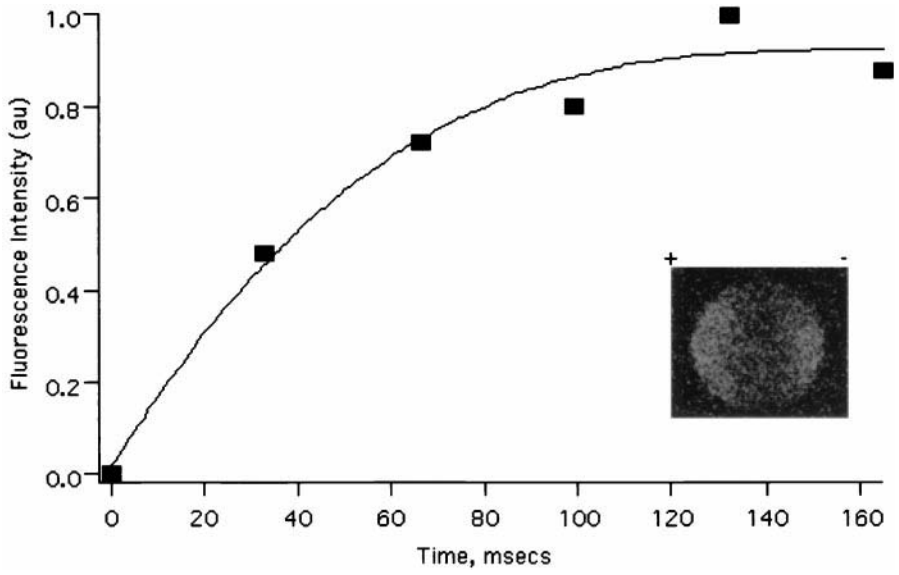

FIGURE 4 Resealing of field-induced membrane pores. The vesicle loaded with Fluo-3 was porated at 500 V/cm, 700-μs pulse duration, in the presence of 2.5 mM $CaCl_2$. The fluorescence intensity from successive video frames as that shown in the inset was integrated and plotted. The solid line is a two-parameter fit based on Eq. 8. The time of resealing from the fit was ~164 ms.

major rearrangement and undulation occurs on the membrane surface as shown in Fig. 2, B' and C'. All the images are from the same vesicle preparation. The field and pulse width were 5.7 kV/cm and 700 μs, respectively. The comparisons in the electron microscope data were gathered from a subpopulation of vesicles with diameters ~1.5–5 μm. Many of the giant vesicles (diameter $\geq$5 μm) were unavailable and possibly disintegrated into the lipid aggregates and other undefined structures seen under the electron microscope. This was observed in both the control and pulsed samples and is due to the blot drying involved in preparing the negatively stained grid samples (see Materials and Methods).

The results shown in Fig. 1 and Fig. 3 establish lipid loss at both hemispheres and that a clear pore is observed at the cathode-facing hemisphere. Whether pores were formed and subsequently resealed at the anode-facing hemisphere was finally assessed by monitoring Ca^{2+} influx from a medium containing 2.5mM $CaCl_2$ into vesicles loaded with Ca^{2+} indicator, Fluo-3. Intact vesicles are impermeable to Ca^{2+} present in the suspending medium. Fig. 4 shows both the rate of Ca^{2+} influx and the spatial permeabilization pattern after an electroporating field of 500 V/cm, 700-μs duration. As shown in the inset of Fig. 4, Ca^{2+} influx occurs at both the anode- and cathode-facing sites indicated by the enhanced fluorescence of Ca^{2+}-Fluo-3 complex. The rate of Ca^{2+} influx is shown in the intensity versus time plot of Fig. 4. The data points were obtained by integrating the fluorescence intensity inside the vesicle from successive video frames at the indicated times and shows a rapid rise followed by a plateau within ~100–200 ms after the pulse. We should mention here that the plateau was neither caused by saturation of the indicator dye nor due to saturation of the camera's detection limit. The observed time course could thus indicate the rate of pore closure of the perforated membrane. The solid line in Fig. 4 is a fit to the data assuming a simple diffusion of Ca^{2+} ions through a time-dependent pore of radius $r = r(t)$ (see Appendix).

Taken together, results presented here show that the pore distribution at the membrane level is asymmetric with large pores at the cathode- and small but numerous pores at the anode-facing hemisphere. The creation of these pores is accompanied with loss of lipid from the membrane surface. We should mention here that the data shown represent results from the majority of the cases we have looked at. In general, unilamellarity of the vesicles was not checked independently but was assessed only by the sharpness of the membrane stain. Heavily multi-layered vesicles, including some with patchy stained surfaces, were easily identifiable, as were those containing other smaller vesicles within them, and were not used for the experiments. In some cases, vesicles simply disintegrated upon field application. However, this does not appear to correlate with the strength of the applied field used as many others were found to sustain much higher field strengths. In general, experiments were carried out at ~1–1.5 V over what we estimated to be a critical permeabilization potential, $\Delta\phi_c$, of 648 mV. Fig. 5 shows a linear plot of Eq. 1, whose slope gives $\Delta\phi_c$. The data points in the figure were determined from the minimum field strength experimentally required to observe Ca^{2+} influx into Fluo-3-loaded vesicles. The electric field strength was incremented at 50 V/cm.

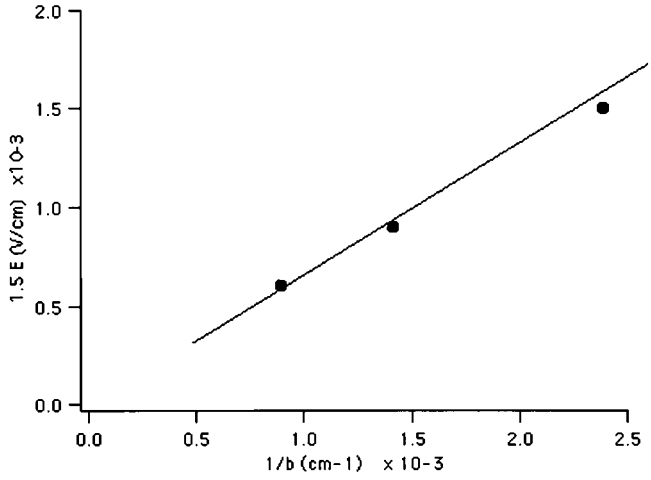

FIGURE 5 Determination of the critical permeabilization potential, $\Delta\phi_c$. The critical potential is defined as the minimum potential required for observable pore formation. This value was determined from three vesicle sizes based on the transport of Ca^{2+} ions into Fluo-3-loaded vesicles. The electric field was incremented at 50 V/cm. The field strength is plotted against the inverse of the vesicle radius and considering $\cos(\theta) = 1$ (see Eq. 1). The slope of the fitted line gives $\Delta\phi_c = 648$ mV.

DISCUSSION

The effect of an externally applied electric field on the integrity of cell membranes in many cell types and vesicles, as well as planar lipid bilayer systems, has been studied by means of a wide variety of methods, including conductometric, optical, and rapid freezing techniques. The most consistent finding in all systems investigated has been the rupture of membranes provided sufficient field strength is applied. Elegant studies using sea urchin eggs (Hibino et al., 1993) and hemispherical bilayer vesicles (Lojewska et al., 1989) have shown that the temporal and spatial variations of the membrane potential due to external fields behaves as predicted by theory. However, how and where the membrane ruptures to challenges of an excess potential have produced differing results and interpretations.

Induction of membrane pores at some critical potential implies that both hemispheres of the vesicle (cell) facing the electrodes be permeabilized. To date, an apparent symmetric permeabilization has been shown only when bipolar pulses were used (Tekle et al., 1991). The asymmetry often observed in many transport studies is believed to originate due to a resting transmembrane potential in cells (negative inside), thereby making the hemisphere facing the anode more susceptible to rupture. However, this same hypothesis was used to explain the susceptibility of the cathode-facing hemisphere, because poration on one side can conceivably double the potential on the opposite side. Teruel and Meyer (1997) proposed unequal distribution of charged phospholipid components at the membrane level to explain asymmetric Ca^{2+} entry in depolarized cells, and more recently ionic concentration gradients have been suggested to influence the creation of asymmetric pore populations (DeBruin and Krassowska, 1999a). Despite these interesting propositions, the asymmetry in electroporation still remains even under conditions where large fields are applied that could easily overwhelm the relatively small transmembrane potentials across cell membranes (Tekle et al., 1990) or even under conditions where, as shown in the present study, neither a resting membrane potential, uneven lipid distribution, nor ionic species exist in the vesicle preparations used. This last point suggests other additional factors are probably involved in determining the perforation pattern.

It is likely the pore distribution observed on the time scale of our detection system results from a complex set of lipid rearrangements that continues after the external field is turned off. One possible initial source of asymmetry may, however, reside on how the external electric field interacts with the intrinsic dipole potentials in the inner and outer layer of the membrane bilayer (Loew, 1993). The dipole potential is the potential difference between the center of the bilayer and the membrane/water interface, and its magnitude has been reported to be of the order of ~300–450 mV (Gross et al., 1994; Reyes et al., 1983). The electric field generated from these dipoles is directed from the center of the bilayer toward the surface of the inner and outer lipid layers. Considering that there would be more lipids on the outer leaflet than on the inner leaflet due to packing constraints, it is possible to imagine a net field could exist directed toward the vesicle surface. If this mechanism is operative, it could result in a larger potential drop at the cathode-facing hemisphere compared with that of the anode and may play a part in the induction of the large pores observed at the negative electrode. Although this is currently speculative, it should be possible to test this hypothesis by using factors that could modulate the dipole potential. Additionally, faster detection systems would also offer capturing events at earlier times and shade light to the evolution of the pore structures observed here.

The processes leading to the induction of pores and the resulting structure and distribution found here may in fact be common to other previously studied cellular systems for a number of reasons. As shown in Fig. 5, the magnitude of the critical potential required for permeabilization (~0.6 V) measured by Ca^{2+} influx, is similar to that found in many cellular systems, typically in the range of 0.5–1.0 V. Secondly, influx studies of a number of fluorescent indicator dyes of varying charge and size has previously been shown to be selective (Tekle et al. 1994; Gabriel and Teissie, 1997). These selective transport patterns are consistent with the pore distributions found here at the membrane level. In other systems where asymmetry is observed, it is important to note that it may not necessarily indicate the state of pore population at the membrane level. Transport through a single large pore versus that which takes place through many small pores spread over a wide region may lead to the mistaken conclusion that one side is more porated than the

other. As is shown in the analysis of the lipid loss due to pore formation in the present system, the total porous area at the two hemispheres could be quite similar despite the fact that the size of the pores is markedly different (Fig. 1 and Table 1). It is, however, possible that such equivalence may not exist at times earlier than we can detect with our system.

The other important finding in this study is the demonstration that lipid loss is associated with pore formation (Figs. 1 and 3 and Table 1). This has not been observed in cellular systems and may be due to the presence of cytoskeletal and other protein components that may serve as anchors to stabilize the lipid domains of the membrane. The electron micrographs of Fig. 3 clearly show that massive restructuring of the membrane occurs due to electroporation. Although some lipid components are lost, other small cluster of aggregates remain attached to the parent vesicle membrane. We should mention here that analogous loss of lipid components due to external electric field has been implicated in an earlier study of electric birefringence of a three-component, sodium *bis*(2-ethylhexyl)-sulfosuccinate/isooctane/H_2O, reverse micelle system (Tekle and Schelly, 1994).

In summary, we have presented data on the induction and distribution of membrane pores in DOPC vesicles showing asymmetric distribution of pores at the membrane level with large single pores at the cathode- and many small pores at the anode-facing hemisphere, with resultant partial loss of the membrane lipid. The porous areas at the two hemispheres were, however, comparable, and the pores were shown to reseal within a few hundred milliseconds after the pulse.

APPENDIX

The overall pore closure time can be estimated based on Fick's law of two-compartment diffusion (Batschelet, 1971). In general, the rate of mass accumulation $m(t)$ inside an enclosure through a time-dependent pore of radius $r = r(t)$ can be written as

$$\frac{dm}{dt} = 2\pi \int_0^{r(t)} k(C_o - C_i) r dr, \tag{5}$$

where k is the permeability coefficient and C_o, C_i are the concentrations of diffusant (i.e., Ca^{2+} ions in this case) outside and inside the vesicle, respectively. Integrating the right side of Eq. 5, assuming k, C_o are constant and $C_i \ll C_o$, gives

$$\frac{dm}{dt} = kC_0 \pi r^2(t). \tag{6}$$

In the simplest case, we assumed a pore radius function $r(t)$, where the radius shrinks linearly starting at R when $t = 0$ to 0 when $t = T$; i.e.,

$$r(t) = R\left(1 - \frac{t}{T}\right) \tag{7}$$

Substituting $r(t)$ in Eq. 6 with Eq. 7 and integrating, we get the time-dependent accumulation of Ca^{2+} ions in the vesicles as

$$m(t) = k'\left[t - \frac{t^2}{T} + \frac{t^3}{3T^2}\right], \tag{8}$$

where k' is a constant equal to $kC_o\pi R^2$. The solid line in Fig. 3 is a two-parameter fit to the data based on Eq. 8 and gives an overall pore closure time of ~164 ms.

We thank Dr. Blair Bowers for taking the electron microscope data

REFERENCES

Al-Atabee, J. S., B. J. Mulligan, and J. B. Powers. 1990. Interspecific somatic hybrides of rudbeckia-hirta and r-laciniata (compositae). *Plant Cell Rep.* 8:517–520.

Angelova, M. I., S. Soleau, Ph. Meleard, J. F. Faucon, and P. Bothorel. 1992. Preparation of giant vesicles by external AC electric fields, kinetics and applications. *Prog. Colloid Polym Sci.* 89:127–131.

Batschelet, E. 1971. Biomathematics for Life Scientists, Vol.2. Springer-Verlag, New York. 295–297.

Chang, D. C., B. M. Chassy, J. A. Saunders, and A. E. Sowers, editors. 1992. Guide to Electroporation and Electrofusion. Academic Press, New York.

Chang, D. C., and T. S. Reese. 1990. Changes in membrane structure induced by electroporation as revealed by rapid freezing electron microscopy. *Biophys. J.* 58:1–12.

DeBruin, K. A., and W. Krassowska. 1999a. Modeling electroporation in a single cell. II. Effect of ionic concentrations. *Biophys. J.* 77: 1213–1224.

DeBruin, K. A., and W. Krassowska. 1999b. Modeling electroporation in a single cell. I. Effect of field strength and rest potential. *Biophys. J.* 77:1225–1233.

Dimitrov, D. S., and A. E. Sowers. 1990. Membrane electroporation: fast molecular exchange by electroosmosis. *Biochim. Biophys. Acta.* 1022: 381–392.

Ehrenberg, B., D. L. Farkas, E. N. Fluhler, Z. Lojewska, and L. M. Loew. 1987. Membrane potential induced by external electric field pulses can be followed with a potentiometric dye. *Biophys. J.* 51:833–837.

Gabriel, B., and J. Teissie. 1997. Direct observation in the millisecond time range of fluorescent molecule asymmetrical interaction with electropermeabilized cell membrane. *Biophys. J.* 73:2630–2637.

Gabriel, B., and J. Teissie. 1998. Mammalian cell electropermeabilization as revealed by millisecond imaging of fluorescence changes of ethidium bromide in interaction with the membrane. *Bioelectrochem. Bioenerg.* 47:113–118.

Gross, E., R. S. Bedlack, Jr., and L. M. Loew. 1994. Dual-wavelength ratiometric fluorescence measurement of the membrane dipole potential. *Biophys. J.* 67:208–216.

Heller, R., M. J. Jaroszeski, L. F. Glass, J. L. Messina, D. P. Rapaport, R. C. DeConti, N. A. Fenske, R. A. Gilbert, L. M. Mir, and D. S. Reintgen. 1996. PhaseI/II trail for the treatment of cutaneous and subcutaneous tumors using electrochemotherapy. *Cancer.* 77:964–971.

Hibino, M., H. Itoh, and K. Kinosita, Jr. 1993. Time course of cell electroporation as revealed by submicrosecond imaging of transmembrane potential. *Biophys. J.* 64:1789–1800.

Hibino, M., M. Shigemori, H. Itoh, K. Nagayama, and K. Kinosita, Jr. 1991. Membrane conductance of electroporated cell analyzed by submicrosecond imaging of transmembrane potential. *Biophys. J.* 59: 209–220.

Kakorin, S., and E. Neumann. 1998. Kinetics of the electroporative deformation of lipid vesicles and biological cells in an electric field. *Ber Bunsenges Phys. Chem.* 102:670–675.

Kakorin, S., E. Redeker, and E. Neumann. 1998. Electroporative deformation of salt filled lipid vesicles *Eur. Biophys. J.* 27:43–53.

Kakorin, S., S. P. Stoylov, and E. Neumann. 1996. Electro-optics of membrane electroporation in diphenylhexatriene-doped lipid bilayer vesicles. *Biophys. Chem.* 58: 109–116.

Kinosita, K., Jr., I. Ashikawa, N. Saita, H. Yoshimura, H. Itoh, K. Nagayama, and K. Ikegami. 1988. Electroporation of cell membrane visualized under a pulsed-laser fluorescence microscope. *Biophys. J.* 53: 1015–1019.

Loew, L. M. 1993. The electrical properties of biomembranes. *In* Biomembranes. Physical Aspects. M. Shinitzky, editor. VCH Publishers, Weinheim, Germany. 341–371.

Lojewska, Z., D. L. Farkas, B. Ehrenberg, and L. M. Loew. 1989. Analysis of the effect of medium conductance on the amplitude and kinetics of the membrane potentials induced by externally applied electric fields. *Biophys. J.* 56:121–128.

Mehrle, W., U. Zimmermann, and R. Hampp. 1985. Evidence for the asymmetrical uptake of fluorescent dyes through electropermeabilized membranes of avena mesophyll protoplasts. *FEBS Lett.* 185:89–94.

Mehrle, W., R. Hampp, and U. Zimmermann. 1989. Electric pulse induced membrane permeabilization. Spatial orientation and kinetics of solute efflux in freely suspended and dielectrophoretically aligned plan mesophyll protoplasts. *Biochim. Biophys. Acta.* 978:267–275.

Miller, J. F., W. J. Dower, and L. S. Tompkins. 1988. High-voltage electroporation of bacteria-genetic transformation of Campylobacter jejuni with plasmid DNA. *Proc. Natl. Acad. Sci. U. S. A.* 85:856–860.

Moscho, A., O. Orwar, D. T. Chiu, B. P. Modi, and R. N. Zare. 1996. Rapid preparation of giant unilammelar vesicles. *Proc. Natl. Acad. Sci.* USA 93:11443–11447.

Mouneimne, Y., P. F. Tosi, R. Barhoumi, and C. Nicolau. 1991. Electroinsertion of xeno proteins in red blood cell membranes yields a long lived protein carrier in circulation. *Biochim. Biophys. Acta.* 1066:83–89.

Newmann, E., A. E. Sowers, and C. A. Jordan, editors. 1989. Electroporation and Electrofusion in Cell Biology. Plenum Press, New York.

Neumann, E., and K. Rosenheck. 1973. Potential difference across vesicular membranes. *J. Membr. Biol.* 14:194–196.

Neumann, E., K. Toensing, S. Kakorin, P. Budde, and J. Frey. 1998. Mechanism of electroporative dye uptake by mouse B cells *Biophys. J.* 74:98–108.

Potter, H. 1988. Electroporation in biology: methods, applications, and instrumentation. *Anal. Biochem.* 174:361–373.

Prausnitz, M. R., V. G. Bose, R. Langer, and J. C. Weaver. 1993. Electroporation of mammalian skin: mechanism to enhance transdermal drug delivery. *Proc. Natl. Acad. Sci. U. S. A.* 90:10504–10508.

Reyes, J., F. Greco, R. Motais, and R. Latorre. 1983. Phloretin and phloretin analogs: mode of action in planar lipid bilayers and monolayers. *J. Membr. Biol.* 72:93–103.

Saulis, G. 1993. Theoretical investigation of the appearance of asymmetric distribution of pores on the cell and their further evolution. *Bioelectrochem. Bioenerg.* 32:249–265.

Saulis, G., M. S. Venslauskas, and J. Naktinis. 1991. Kinetics of pore resealing in cell membranes after electroporation. *Bioelectrochem. Bioenerg.* 26:1–13.

Sowers. A. E. 1987. The long lived fusogenic state induced in erythrocyte ghosts by electric pulses is not laterally mobile. *Biophys. J.* 52: 1015–1029.

Sowers, A. E., and M. R. Lieber. 1986. Electropore diameters, lifetimes, numbers, and locations in individual erythrocyte ghosts. *FEBS Lett.* 205:179–184.

Sugar, I. P., and E. Neumann. 1984. Stochastic model for electric field induced membrane pores: electroporation. *Biophys. Chem.* 19:211–225.

Teissie, J., and T. Y. Tsong. 1981. Electric field induced transient pores in phospholipid bilayer vesicles. *Biochemistry.* 20:1548–1554.

Tekle, E., R. D. Astumian, and P. B. Chock. 1990. Electro-permeabilization of cell membranes: effect of the resting membrane potential. *Biochem. Biophys. Res. Commun.* 172:282–287.

Tekle, E., R. D. Astumian, and P. B. Chock. 1991. Electroporation by using bipolar oscillating electric field: an improved method for DNA transfection of NIH3T3 cells. *Proc. Natl. Acad. Sci. U. S. A.* 88:4230–4234.

Tekle, E., R. D. Astumian, and P. B. Chock. 1994. Selective and asymmetric molecular transport across electroporated cell membranes. *Proc. Natl. Acad. Sci. U. S. A.* 91:11512–11516.

Tekle, E., and Z. A. Schelly. 1994. Modeling the electric birefringence relaxations of AOT/Isooctane/H_2O water-in-oil microemulsions. *J. Phys. Chem.* 98:7657–7664.

Teruel, M. N., and T. Meyer. 1997. Electroporation-induced formation of individual calcium entry sites in the cell body and processes of adherent cells. *Biophys. J.* 73:1785–1789.

Tonsing, K., S. Kakorin, E. Neumann, S. Liemann, and R. Huber. 1997. Annexin V and vesicle membrane electroporation *Eur. Biophys. J.* 26:307–318.

Tsong, T. Y. 1991. Electroporation of cell membranes. *Biophys. J.* 60: 297–306.

Weaver, J. C., and A. Barnett. 1992. Progress towards a theoretical model for electroporation: membrane electrical behavior and molecular transport. *In* Guide to Electroporation and Electrofusion. D. C. Chang, B. M. Chassy, J. A. Saunders, and A. E. Sowers, editors. Academic Press, New York. 91–118.

Zhelev, D. V., and D. Needham. 1993. Tension-stabilized pores in giant vesicles: determination of pore size and pore line tension. *Biochim. Biophys. Acta.* 1147:89–104.

Zimmermann, U. 1986. Electrical breakdown, electropermeabilization and electrofusion. *Rev. Physiol. Biochem. Pharmacol.* 105:175–256.